


Article

# Comparison of Continuous In-Situ CO<sub>2</sub> Measurements with Co-Located Column-Averaged XCO<sub>2</sub> TCCON/Satellite Observations and CarbonTracker Model Over the Zugspitze Region

Ye Yuan <sup>1,\*</sup>, Ralf Sussmann <sup>2</sup>, Markus Rettinger <sup>2</sup>, Ludwig Ries <sup>3</sup> , Hannes Petermeier <sup>4</sup> and Annette Menzel <sup>1,5</sup>

<sup>1</sup> Department of Ecology and Ecosystem Management, Technical University of Munich, 85354 Freising, Germany; annette.menzel@tum.de

<sup>2</sup> Karlsruhe Institute of Technology, IMK-IFU, 82467 Garmisch-Partenkirchen, Germany; ralf.sussmann@kit.edu (R.S.); markus.rettinger@kit.edu (M.R.)

<sup>3</sup> German Environment Agency (UBA), GAW Global Observatory Zugspitze-Hohenpeissenberg, 82475 Platform Zugspitze, Germany; ludwig.ries@gawstat.de

<sup>4</sup> Department of Mathematics, Technical University of Munich, 85748 Garching, Germany; hannes.petermeier@tum.de

<sup>5</sup> Institute for Advanced Study, Technical University of Munich, 85748 Garching, Germany

\* Correspondence: yuan@wzw.tum.de

Received: 13 November 2019; Accepted: 11 December 2019; Published: 12 December 2019



**Abstract:** Atmospheric CO<sub>2</sub> measurements are important in understanding the global carbon cycle and in studying local sources and sinks. Ground and satellite-based measurements provide information on different temporal and spatial scales. However, the compatibility of such measurements at single sites is still underexplored, and the applicability of consistent data processing routines remains a challenge. In this study, we present an inter-comparison among representative surface and column-averaged CO<sub>2</sub> records derived from continuous in-situ measurements, ground-based Fourier transform infrared measurements, satellite measurements, and modeled results over the Mount Zugspitze region of Germany. The mean annual growth rates agree well with around 2.2 ppm yr<sup>-1</sup> over a 17-year period (2002–2018), while the mean seasonal amplitudes show distinct differences (surface: 11.7 ppm/column-averaged: 6.6 ppm) due to differing air masses. We were able to demonstrate that, by using consistent data processing routines with proper data retrieval and gap interpolation algorithms, the trend and seasonality can be well extracted from all measurement data sets.

**Keywords:** carbon dioxide; XCO<sub>2</sub>; in situ; remote sensing; satellite; time-series analysis; seasonality

## 1. Introduction

Atmospheric carbon dioxide (CO<sub>2</sub>) is the most important anthropogenic greenhouse gas and has increased globally from around 280 parts per million (ppm) since 1850 to over 400 ppm nowadays [1,2]. Measurements of atmospheric CO<sub>2</sub> are performed over the globe and via different measurement techniques. To derive precise CO<sub>2</sub> concentrations at the Earth's surface, representative of lower free tropospheric conditions, continuous in-situ measurements are made with high temporal resolution at either representative ground-based measurement sites or tall towers. Depending on the location, surface measurement sites can provide long-term records that are representative of regional and global scales, e.g., stations within the Global Atmosphere Watch (GAW) network [3]. In addition, to estimate the column-averaged mole fractions of CO<sub>2</sub> (XCO<sub>2</sub>), remote-sensing techniques have been operated

at various sites via ground-based Fourier transform infrared (FTIR) measurements within the Total Carbon Column Observing Network (TCCON; [4]). Measurements of such global networks can thus be compared with each other and can be exploited for further use, such as the validation of satellite data and as a-priori input for models. Unlike ground-based measurement systems, satellites are capable of collecting data on the global scale with different spatial and temporal coverages, such as the Greenhouse Gases Observing Satellite (GOSAT; [5]) and the Orbiting Carbon Observatory-2 (OCO-2; [6]). Models, however, can take measurements into account and estimate with regard to only the concentrations global flux exchanges between the surface and atmosphere by simulating the atmospheric transport. As a result, the global carbon cycle could be better understood if all measurement techniques are evaluated and compared.

Many analyses have focused on regional and global surface CO<sub>2</sub> concentrations from selected in-situ measurements. Atmospheric CO<sub>2</sub> records at several central European mountain stations were evaluated, showing their improved representativeness on the CO<sub>2</sub> background levels after data selection [7]. In China, continuous measurements at four GAW regional and global stations were also analyzed, focusing on the characteristics of sampling sites and the influence of local sources [8]. Moreover, remote sites can serve as reference stations in urban studies. A comparison was made for a long-term CO<sub>2</sub> time-series measured from Southwest London with the CO<sub>2</sub> measurements at Mace Head, Ireland, exhibiting a higher growth rate and larger seasonal amplitudes, driven greatly by the anthropogenic emissions [9]. At the same time, inter-comparisons among satellites and cross-validations with ground-based FTIR have also frequently been made. A multi-year comparison of XCO<sub>2</sub> from Scanning Imaging Absorption Spectrometer for Atmospheric Cartography (SCIAMACHY; [10,11]), GOSAT, and Atmospheric Infrared Sounder (AIRS; [12]) was performed with the validation reference of TCCON measurements, and revealed that AIRS data products showed a better performance in both coverage and accuracy [13]. A further study of the comparison of GOSAT and OCO-2 reported that, despite the CO<sub>2</sub> detection capabilities in both satellites, OCO-2 performed better in detection coverage and spatial resolution [14].

However, so far, less attention has been paid to the differences between surface and column measurements at single sites. Column CO<sub>2</sub> from Fourier transform spectrometer was found to be similar to surface CO<sub>2</sub> concentrations from flask, tower, and aircraft observations regarding the amplitude of diurnal and seasonal cycles, but with less variability at both spatial and temporal scales [15]. However, this study focused more on the general patterns resulting from an atmospheric transport model instead of on characteristics of point measurements. However, a systematic comparison was performed at Jungfraujoch, Switzerland, on the in-situ Nondispersive Infrared Analyzer (NDIR) and column FTIR measurements, revealing similar differences in the seasonality (column about one half of surface), but differences that are consistent in the annual CO<sub>2</sub> increase with high correlation [16]. Still, no satellite or model-based results were included. Nevertheless, there were two studies with seasonal and spatial focuses, comparing satellite measurements with ground-based measurements over East Asia and Indian regions [17,18]. In Europe, only the Scanning Imaging Absorption Spectrometer for Atmospheric Cartography sensor (SCIAMACHY) and CO<sub>2</sub> ground measurements at a rural site in the upper Spanish plateau were compared, showing similar seasonal patterns and a satisfying agreement between inter-annual trends, but only with a short studied time period [19]. Surface and column CO<sub>2</sub> data were compared at Ny-Alesund, and a smaller amplitude in the column was found [20]. This was explained by the fact that the processes responsible for the seasonality, namely plant photosynthesis sinks and plant and microbial respiration, take place at the Earth's surface. Besides, co-located column and in-situ CO<sub>2</sub> measurements in the tropics were compared with atmospheric tracer transport model TM3 simulations, which resulted in a good agreement [21].

In this study, we intend to answer the following research questions using a set of CO<sub>2</sub> time-series derived from surface/column-averaged measurements performed in the Zugspitze region of Southern Germany.

1. Can a consistent data processing routine be successfully applied to both continuous in-situ and column-averaged CO<sub>2</sub> measurements for comparisons with increased representativeness?
2. Are the surface and satellite measurements comparable even though they are representative of a single measurement site or a designated region/column average?
3. If significant differences are detected, what are the specific differences in annual growth rates and seasonal amplitudes?

The sections below are organized as follows. Section 2 gives a general description of the CO<sub>2</sub> series. Details in the data processing routine and analyses are given in Section 3. Results and discussion regarding the trend and seasonality are presented in Sections 4 and 5, followed by conclusions on their comparability and applicability in Section 6.

## 2. CO<sub>2</sub>/XCO<sub>2</sub> Data Sets

### 2.1. Surface In-Situ Measurements

The long-term surface CO<sub>2</sub> records (2002–2018) measured at the GAW global station Zugspitze–Schneefernerhaus, Germany (GAW ID: ZSF) were used in this study. The location of ZSF is at the Southern slope of Mount Zugspitze (47.42°N, 10.98°E) at an elevation of 2670 m above sea level (a.s.l.). Measurements of atmospheric CO<sub>2</sub> at Zugspitze had already started in the 1980s, but were re-located to this research station in 2001. The complete and validated CO<sub>2</sub> time-series has been available since 2002, and thus was used here as CO<sub>2</sub>\_INSITU\_ZSF. For more detailed information regarding the site and experimental instruments, we refer the reader to Yuan et al. [22].

### 2.2. TCCON

TCCON is the network of ground-based FTS measuring the column-averaged concentrations of atmospheric components such as CO<sub>2</sub> and CH<sub>4</sub> by recording the solar absorption spectra in the near-infrared [23]. Two measurement sites were chosen close to ZSF, i.e., the TCCON sites Garmisch (47.48°N, 11.06°E, 743 m a.s.l.) and Zugspitze (47.42°N, 10.98°E, 2964 m a.s.l.), equipped with the Bruker IFS125HR spectrometer [24]. The data version GGG2014 was used, which is available at <https://tccodata.org/> [25,26]. Temporal coverage was different since XCO<sub>2</sub> time-series have been available at Garmisch since 2007 and at Zugspitze since 2015. The column-averaged dry air mole fractions of CO<sub>2</sub> were extracted in ppm, denoted as XCO<sub>2</sub>\_TCCON\_Garmisch and XCO<sub>2</sub>\_TCCON\_Zugspitze.

### 2.3. Satellite

Satellite data were taken from a merged CO<sub>2</sub> satellite product described in Buchwitz et al. [27] (available at <https://cds.climate.copernicus.eu/>) from the Scanning Imaging Absorption Spectrometer for Atmospheric Cartography sensor (SCIAMACHY) on the Environmental Satellite (ENVISAT) from 2002 to 2012, and the subunit Fourier Transform Spectrometer of the Thermal And Near-infrared Sensor for carbon Observation sensor (TANSO-FTS) on the GOSAT since 2009, referred to as XCO<sub>2</sub>\_SAT\_Obs4MIPs. To make the satellite XCO<sub>2</sub> time-series more comparable with in-situ measurements on the temporal scale, measurements from the OCO-2 satellite launched and operated since July 2014 were further included [28]. For this study, XCO<sub>2</sub> data from the OCO-2 9 lite product were derived from the CO<sub>2</sub> Virtual Science Data Environment in the Jet Propulsion Laboratory, California Institute of Technology (<https://co2.jpl.nasa.gov/>), abbreviated as XCO<sub>2</sub>\_SAT\_OCO-2. Again, measurements were extracted as column-averaged dry air mole fractions of CO<sub>2</sub>.

### 2.4. CarbonTracker

CarbonTracker ([29], with updates documented at <http://carbontracker.noaa.gov>), the global CO<sub>2</sub> modeling system developed by National Oceanic and Atmospheric Administration Earth System Research Laboratory (NOAA ESRL, USA), was used for validation purposes. It assimilates almost

400 time-series from real CO<sub>2</sub> observations combining both in-situ continuous and flask measurements from the surface, as well as tower, aircraft, and shipboard measurements. The current version CT2017 provides modeled CO<sub>2</sub> mole fractions from 2000 to 2016. For modeling the CO<sub>2</sub> mole fractions for a longer time period, CarbonTracker Near-Real Time (version CT-NRT.v2018-1), which is an extension of CT2017 using real-time meteorology and a different prior flux model with assimilations of fewer CO<sub>2</sub> observations, was chosen. These two data sets were named CO<sub>2</sub>\_CT2017 and CO<sub>2</sub>\_CT-NRT.v2018-1, respectively. Figure 1 shows the overall map of measurement sites and sampling grids for all data sets used in the study.

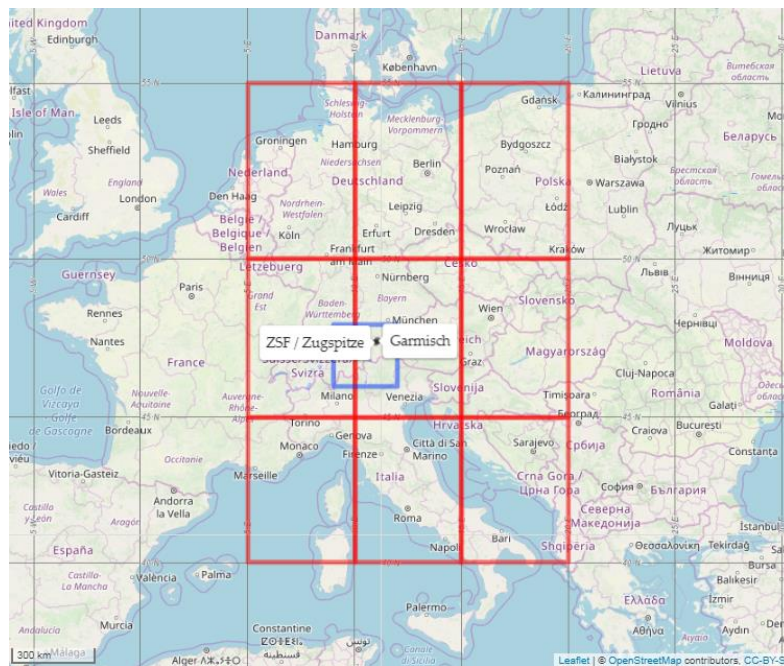


**Figure 1.** Locations of GAW Global station ZSF and TCCON sites Zugspitze and Garmisch with rectangles representing the spatial coverage of XCO<sub>2</sub> levels extracted in this study for satellite measurements (red) and CarbonTracker-modeled results (blue).

### 3. Methods

#### 3.1. Data Integration

For a complete and consistent analysis, all data sets were first collected and averaged to monthly values. The surface continuous data set CO<sub>2</sub>\_INSITU\_ZSF used here consisted of 30 min averages from 2002 to 2018, and thus all other data sets were selected in the same corresponding time period. Regarding the TCCON network, agreements in daily measurements between Garmisch and Zugspitze were examined by calculating their difference (XCO<sub>2</sub>\_TCCON\_Garmisch minus XCO<sub>2</sub>\_TCCON\_Zugspitze) for the overlapping time period (April 2015–December 2018). A mean daily difference of  $-0.24 \pm 1.32$  ppm (one standard deviation) was derived within the accuracy of 0.2% for the TCCON measurements [30]. Therefore, both data sets were included, but the XCO<sub>2</sub>\_TCCON\_Garmisch data set was used, starting in 2008 due to only 6 months of data being available in 2007.

For satellite measurements, Level 3 product Obs4MIPs Version 3.0 on a monthly scale was first chosen over 2003–2016. To derive the best appropriate mole fractions comparable to the other point measurements, the centered and surrounding eight grids of the Zugspitze region were collected (see Figure 1) and averaged as XCO<sub>2</sub> levels, representative of a broader region and which due to a large amount (34.5%) of missing values at the centered grid. However, the OCO-2 satellite measurements were selected with the customized time period of 2017–2018 and integrated into Level 3 gridded monthly data set with the same spatial and temporal resolutions as XCO<sub>2</sub>\_sat\_Obs4MIPs by the same data



averaging from the centered and surrounding grids. Later, these two satellite data sets were merged and denoted as XCO<sub>2</sub>\_SAT\_merge.

The validation CarbonTracker model data sets were integrated in the following ways. As recommended by NOAA (<https://www.esrl.noaa.gov/gmd/ccgg/carbontracker/CT-NRT/>), the 3 hourly CT2017 data set was used from 2002 to 2016, followed by the CT-NRT.v2018-1 data set used from 2017 to 2018. The inter-comparison between the measurement data sets and the CarbonTracker model was reliable since CO<sub>2</sub>\_INSITU\_ZSF was not included in the CarbonTracker Observational Network. Additionally, the modeled results were representative of different measurement heights because the implemented Transport Model 5 (TM5) used a 25-layer subset in the vertical of ERA-interim transport [31]. We only extracted the modeled CO<sub>2</sub> concentrations at the centered grid (see Figure 1) averaged from Levels 6 to 10 (about 1.2 km to 5.5 km above the ground) as the “free troposphere” (FT, indicated at <https://www.esrl.noaa.gov/gmd/ccgg/carbontracker/index.php>), as well as the total column averages (Levels 1 to 25), representative of XCO<sub>2</sub> concentrations at both Garmisch and Zugspitze. Thus, the overall modeled data sets for comparison are referred to as CO<sub>2</sub>\_CT\_merge\_L6-10 and XCO<sub>2</sub>\_CT\_merge\_L1-25. A comprehensive description of all data sets regarding instrumentation, temporal, and spatial coverage is given in Table 1.

**Table 1.** Information on the CO<sub>2</sub> and XCO<sub>2</sub> data sets used in the study.

Measurement Data Set	Time Period	Spatial Resolution (Lon × Lat)	Temporal Resolution	Instrument	Merged Data Set Used in the Study
CO <sub>2</sub> _INSITU_ZSF	2002–2018	–	half-hourly	GC-FID	CO <sub>2</sub> _INSITU_ZSF; CO <sub>2</sub> _INSITU_ZSF_ADV5
XCO <sub>2</sub> _TCCON_Garmisch	2008–2018	–	daily	Bruker IFS125HR	XCO <sub>2</sub> _TCCON_Garmisch
XCO <sub>2</sub> _TCCON_Zugspitze	2015–2018	–	daily	Bruker IFS125HR	XCO <sub>2</sub> _TCCON_Zugspitze
XCO <sub>2</sub> _SAT_Obs4MIPs	2003–2016	5° × 5°	monthly	SCIAMACHY/TANSO-FTS	XCO <sub>2</sub> _SAT_merge
XCO <sub>2</sub> _SAT_OCO-2	2017–2018	5° × 5°	monthly	OCO-2	
(X)CO <sub>2</sub> _CT2017	2002–2016	3° × 2°	3-hourly	-	CO <sub>2</sub> _CT_merge_L6-10; XCO <sub>2</sub> _CT_merge_L1-25
(X)CO <sub>2</sub> _CT-NRT.v2018-1	2017–2018	3° × 2°	3-hourly	-	

### 3.2. Data Processing

In order to derive the most representative background CO<sub>2</sub> levels for the lower free troposphere from the CO<sub>2</sub>\_INSITU\_ZSF data set, the data selection method ADVS (Adaptive Diurnal minimum Variation Selection) was applied, which has been proven to be valid for European elevated mountain stations [7], and for long-term continuous measurements [22]. With a nighttime starting selection time window statistically identified based on data variability, the ADVS method selects the best appropriate CO<sub>2</sub> data on a daily basis. The selection threshold criterion at ZSF was set to no more than 0.3 ppm (standard deviation) within a 6-hour time window (22:00–03:00 local time). In total, 14.0% of validated 30-min CO<sub>2</sub> data were selected.

For all monthly averaged data sets, cubic spline interpolation was applied to fill missing values in the time-series, mainly for XCO<sub>2</sub>\_SAT\_Obs4MIPs during winter periods (mostly December and January) due to poor data quality (e.g., cloudiness, shadows, or other factors). Subsequently, all CO<sub>2</sub> time-series were decomposed into trend, seasonal, and remainder components for further analysis using Seasonal and Trend decomposition using Loess (STL) [32]. The STL method applies the moving average technique in an inner loop with seasonal and trend smoothers based on Locally Estimated Scatterplot Smoothing (Loess), and an outer loop weighting the fitted values for the next run of smoothing until convergence is reached [33]. The smoothing parameters *s.window* = 5 years and *t.window* = 25 months were chosen for the seasonal and trend components, respectively. A periodic window for seasonal extraction was tested and the result was similar. The remainder of the components were assessed for all records, but no systematic signals were detected, indicating reliable decomposed results for further analysis (see Figure A1). The STL-decomposed trend and seasonal components were combined and are shown as curve fitting for all CO<sub>2</sub>/XCO<sub>2</sub> time-series.

### 3.3. Data Analysis

The CO<sub>2</sub> annual growth rate was calculated from the STL-decomposed trend component based on the definition by NOAA [2], following the instructions in Buchwitz et al. [27]. For each month, we calculated the difference in CO<sub>2</sub> or XCO<sub>2</sub> between this month and the same month from the previous year. Thus, 12 values were calculated for each year. Then, the mean annual growth rate was considered as the mean of these 12 differences. The mean annual growth rates were further used for correlation analysis by Pearson's product moment correlation, with error bars defined by the 95% confidence intervals calculated from averaging the 12 values in each year.

However, the seasonal cycle was determined from the STL-decomposed seasonal component with the seasonal amplitude calculated from the monthly maximum minus the monthly minimum of the year. The calculation method of seasonal amplitude has been compared with the curve fitting technique, by Lindqvist et al. [34] applying a skewed sine wave for the seasonal cycle, resulting in the same values. More details can be found in the Appendix A.

All data processing, analyses, and visualizations in this study were done under R programming environment (version 3.6.0) [35], with the implemented packages data.table [36], openair [37], zoo [38], ggplot2 [39], leaflet [40], mapview [41], grid [35], and gridExtra [42].

## 4. Results

This section first reports the complete CO<sub>2</sub> time-series compared. Then, the results of STL decomposition are shown with inter-annual variations of annual growth rates and seasonal cycles. A statistical summary can be found in Table A1.

### 4.1. Time-Series of CO<sub>2</sub> and XCO<sub>2</sub>

The atmospheric CO<sub>2</sub> and XCO<sub>2</sub> mole fractions from all measurement data sets, including the ADVS-selected surface in-situ time-series CO<sub>2</sub>\_INSITU\_ZSF\_ADVS, are given in Figure 2. All time-series are plotted in monthly resolution, together with the fitted curves that are integrated from STL-decomposed trend and seasonal components. CO<sub>2</sub>\_INSITU\_ZSF, CO<sub>2</sub>\_INSITU\_ZSF\_ADVS, CO<sub>2</sub>\_CT\_merge\_L6-10, and XCO<sub>2</sub>\_CT\_merge\_L1-25 covered the complete time period 2002–2018. The first year 2002 was missing for XCO<sub>2</sub>\_SAT\_merge, while XCO<sub>2</sub>\_TCCON\_Garmisch and XCO<sub>2</sub>\_TCCON\_Zugspitze started comparatively later, in 2008 and 2015, respectively. In general, the CarbonTracker-modeled free tropospheric time-series CO<sub>2</sub>\_CT\_merge\_L6-10 agreed well with the continuous in-situ measurements (both CO<sub>2</sub>\_INSITU\_ZSF and CO<sub>2</sub>\_INSITU\_ZSF\_ADVS). However, CO<sub>2</sub>\_INSITU\_ZSF more frequently exhibited CO<sub>2</sub> concentrations outside the curve fitting and thus represented the local and regional influences, e.g., higher CO<sub>2</sub> concentrations in 2008–2009, 2012–2013, and 2018; lower values in 2013–2014. At the same time, ADVS data selection performed effectively to exclude most of the extreme mean monthly concentrations, except for the lower value in 2005. CO<sub>2</sub>\_INSITU\_ZSF\_ADVS was still more similar in the STL-decomposed trend and seasonal fit to CO<sub>2</sub>\_CT\_merge\_L6-10 than the original CO<sub>2</sub>\_INSITU\_ZSF series.

Regarding column-averaged measurements, there were far less variations in the time-series compared to the surface measurements, since they are representative of the mean CO<sub>2</sub> levels of the whole vertical atmospheric concentration distribution and not only of the surface concentration as the in-situ measurements. The satellite time-series XCO<sub>2</sub>\_SAT\_merge was slightly higher compared to the point measurements XCO<sub>2</sub>\_TCCON\_Garmisch and XCO<sub>2</sub>\_TCCON\_Zugspitze, while the CarbonTracker-modeled column averages XCO<sub>2</sub>\_CT\_merge\_L1-25 showed the opposite. Such deviations could be attributed to differences in the representativeness of the grid values. Unlike TCCON measurements, XCO<sub>2</sub> values averaged from the centered and surrounding grids had the tendency to show a mean XCO<sub>2</sub> level from a much more regional perspective. Additionally, the extracted modeled grid for XCO<sub>2</sub>\_CT\_merge\_L1-25 could potentially cover more vegetation signals that were dominant at lower elevations in the Alpine regions nearby. Additionally, it should be noted that the monthly averages for all XCO<sub>2</sub> measurements might not identically indicate the concentrations for the exact same days.

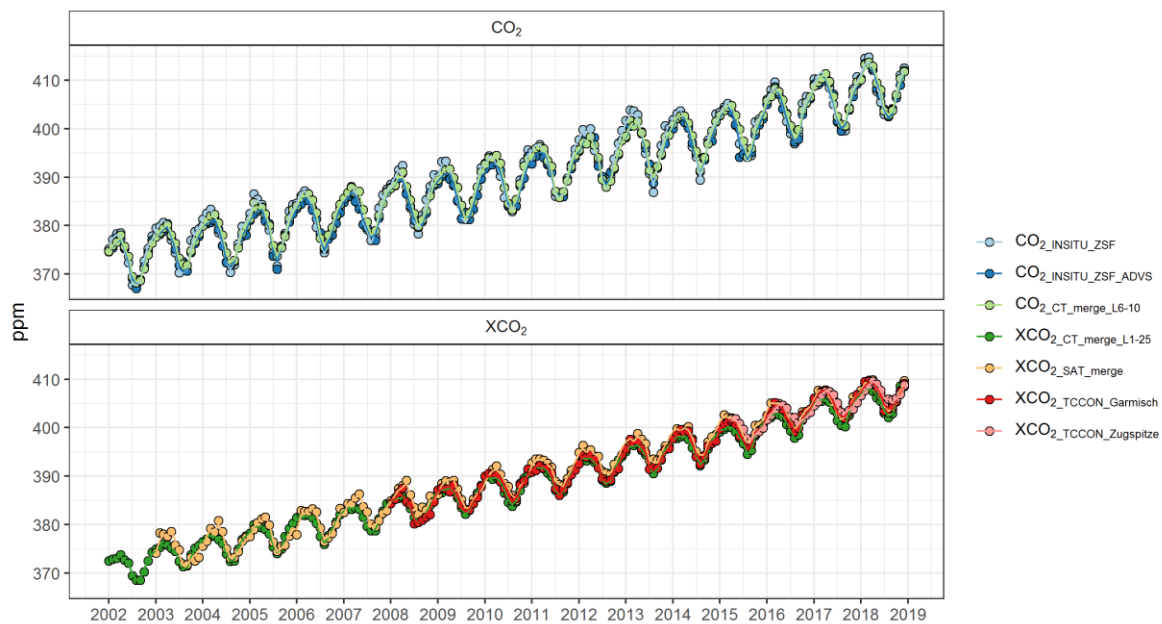


**Figure 2.** Monthly CO<sub>2</sub> series of all measurements/data products shown as colored points with fitted curves (colored lines) consisting of STL-decomposed trend and seasonal components, divided into CO<sub>2</sub> (upper panel) and XCO<sub>2</sub> (lower panel).

Figure 3 shows the offsets of all six data sets with respect to the continuous in-situ ZSF data set (CO<sub>2</sub>\_INSITU\_ZSF), based on the monthly fitted curves. The offsets ranged from  $-5$  to  $5$  ppm with bimodal distributions. All time-series exhibited negative values for the mean monthly differences relative to CO<sub>2</sub>\_INSITU\_ZSF ranging from  $-0.66 \pm 0.15$  ppm (CO<sub>2</sub>\_INSITU\_ZSF\_ADVS) to  $-2.36 \pm 0.32$  ppm (XCO<sub>2</sub>\_CT\_merge\_L1-25), except for CO<sub>2</sub>\_CT\_merge\_L6-10, which showed a positive difference of  $0.01 \pm 0.17$  ppm (see Table A1).

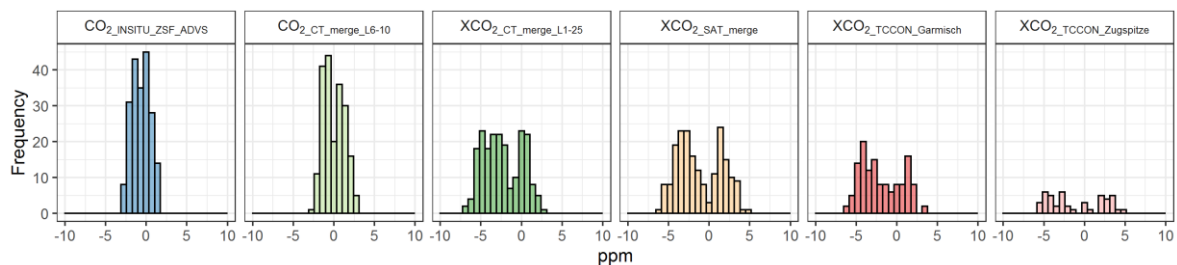


**Figure 3.** Offsets of six different CO<sub>2</sub> and XCO<sub>2</sub> data sets of this study (monthly fitted curves, STL-decomposed trend plus seasonal components) relative to CO<sub>2</sub>\_INSITU\_ZSF.

#### 4.2. Annual Growth Rates

Apart from absolute CO<sub>2</sub> levels, trend analysis is always considered a more promising measure for the comparison of CO<sub>2</sub> time-series, i.e., for assessing whether similar year-to-year increases and inter-annual variations in CO<sub>2</sub> can be detected. The annual CO<sub>2</sub> growth rates are shown as boxplots, together with the mean growth rates connected as lines in Figure 4.

The overall mean annual growth rates of CO<sub>2</sub>\_INSITU\_ZSF ( $2.18 \pm 0.10$  ppm yr<sup>-1</sup>), CO<sub>2</sub>\_INSITU\_ZSF\_ADVS ( $2.20 \pm 0.09$  ppm yr<sup>-1</sup>), and CO<sub>2</sub>\_CT\_merge\_L6-10 ( $2.21 \pm 0.06$  ppm yr<sup>-1</sup>) over 2002–2018 exhibited similar values around 2.2 ppm yr<sup>-1</sup> for the free troposphere, while XCO<sub>2</sub>\_CT\_merge\_L1-25 and XCO<sub>2</sub>\_SAT\_merge (starting 2003) for the total column of the atmosphere increased at slightly lower rates of  $2.15 \pm 0.04$  ppm yr<sup>-1</sup> and  $2.13 \pm 0.06$  ppm yr<sup>-1</sup>, respectively. Due to the late start of TCCON, significantly higher annual growth rates were observed, namely  $2.33 \pm 0.08$  ppm yr<sup>-1</sup> (Garmisch, starting in 2008) and  $2.48 \pm 0.16$  ppm yr<sup>-1</sup> (Zugspitze, starting in 2015).

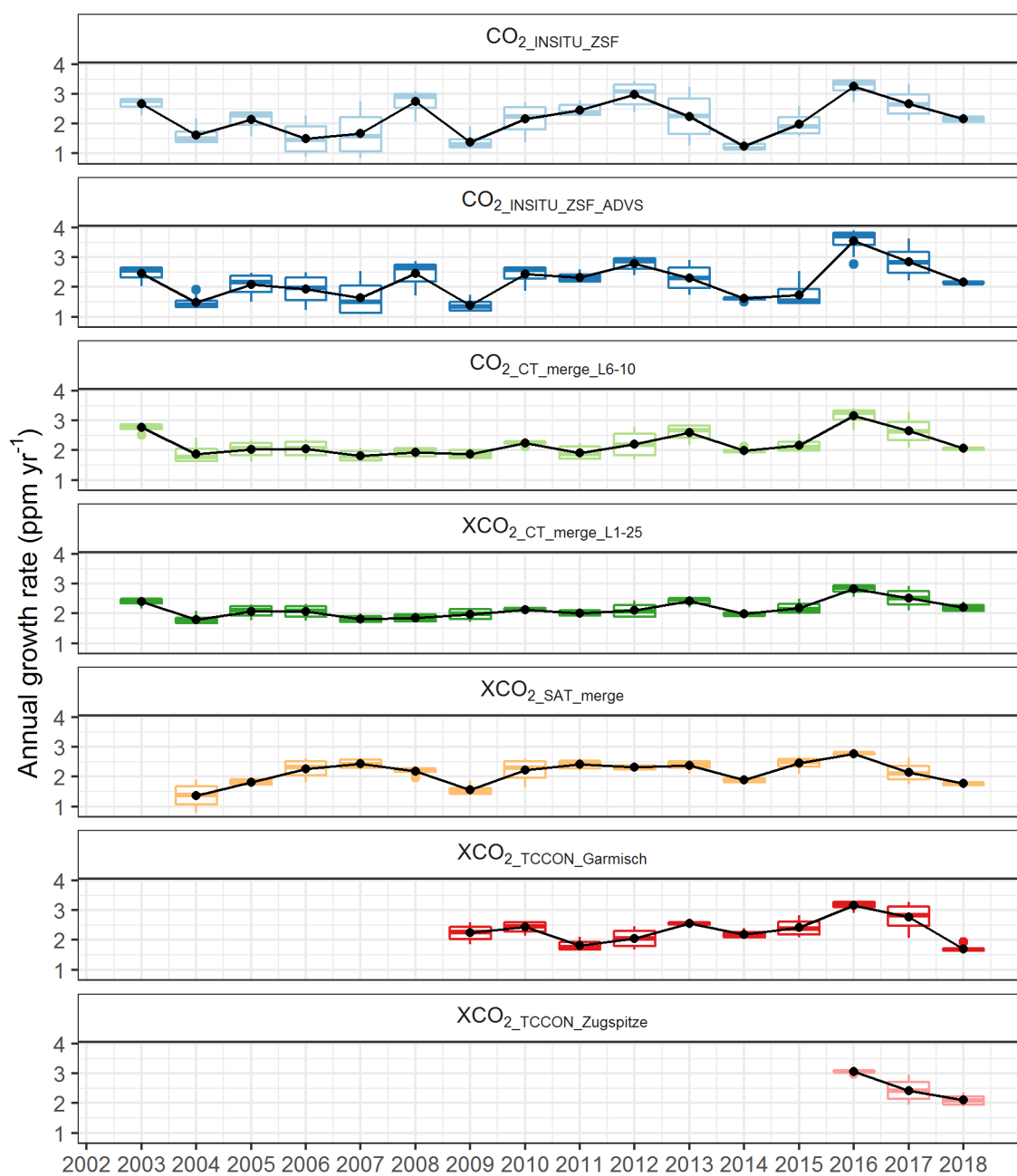


**Figure 4.** Annual mean growth rates derived from all seven CO<sub>2</sub> and XCO<sub>2</sub> series in this study (STL-decomposed trends, black points, and lines). Colored boxplots represent all 12 values of growth rates from monthly averages.

#### 4.3. Seasonal Amplitudes

Seasonal cycles of all CO<sub>2</sub> and XCO<sub>2</sub> time-series were analyzed in regards to whether they followed comparable annual fluctuations and to identify reasons for potential discrepancies. Clear differences were found between continuous in-situ and column-averaged measurements in the mean seasonal peak-to-peak amplitudes, i.e., annual averages of monthly maximum minus monthly minimum, which were calculated from the STL-decomposed seasonal components shown in Figure 5. The largest mean seasonal amplitude of  $13.08 \pm 0.52$  ppm was calculated for CO<sub>2</sub>\_INSITU\_ZSF, indicating a high relevance of local influences at the measurement site. In contrast, the ADVS-selected data set (CO<sub>2</sub>\_INSITU\_ZSF\_ADVS,  $10.93 \pm 0.45$  ppm) agreed well with the modeled CO<sub>2</sub> levels for the free troposphere (CO<sub>2</sub>\_CT\_merge\_L6-10,  $11.05 \pm 0.28$  ppm), supporting a good performance of the CarbonTracker model in simulating the



surface/free tropospheric CO<sub>2</sub> mole fractions. In this circumstance, an estimation of around 2.0 ppm mole fractions of atmospheric CO<sub>2</sub> is assumed to be associated with short-range carbon sources and sinks.

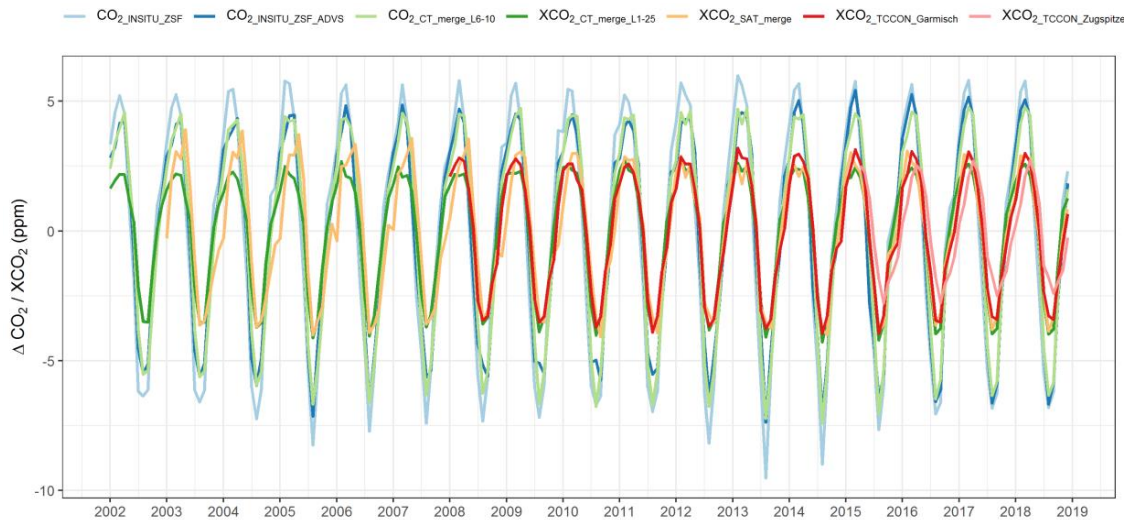


**Figure 5.** Seasonal cycles from STL-decomposed seasonal components of the different CO<sub>2</sub> and XCO<sub>2</sub> series of this study.

## 5. Discussion

The atmospheric CO<sub>2</sub> and XCO<sub>2</sub> mole fractions from all measurement data sets were collected and compared (see Figure 2). The differences between FTIR column observations and continuous in-situ measurements ( $-1.95 \pm 0.43$  ppm for XCO<sub>2</sub>\_TCCON\_Garmisch, and  $-1.03 \pm 1.01$  ppm for XCO<sub>2</sub>\_TCCON\_Zugspitze) were smaller than those found in previous studies, where differences of up to 8% have been reported [20]. This may be explained by the fact that our TCCON column observations were calibrated to World Meteorological Organization (WMO) scale, while the cited column observations were not. Furthermore, the column observations by Schibig et al. [16], showing a difference of 13 ppm with respect to surface measurements at the Jungfrauoch, were performed in the mid-infrared, not in the near-infrared as our TCCON observations. In this context, we note that Buschmann et al. [30] showed that the sensitivity of mid-infrared CO<sub>2</sub> column retrievals is a factor of two lower in the troposphere compared to TCCON-type near-infrared retrievals used in our study.

### 5.1. Inter-Annual Variation in Trend

The STL-decomposed trend components were calculated into annual CO<sub>2</sub> growth rates and overall mean growth rates (see Figure 4). These results perfectly matched those found by Buchwitz et al. [27], who showed a mean difference between the satellite-derived and NOAA CO<sub>2</sub> surface observation annual mean growth rates of  $0.0 \pm 0.3$  ppm yr<sup>-1</sup> ( $\pm 1$  standard deviation). Their reported “record-large” growth rate over 2015–2016 of around 3 ppm yr<sup>-1</sup> due to an El Niño event [43–45] was also clearly observed in all series of our study (ranging from 2.77 to 3.56 ppm yr<sup>-1</sup>).

Equally, inter-annual variations in the annual growth rates were similar for the different CO<sub>2</sub> series. The continuous in-situ measurements (CO<sub>2</sub>\_INSITU\_ZSF and CO<sub>2</sub>\_INSITU\_ZSF\_ADVS) and CarbonTracker free tropospheric model (CO<sub>2</sub>\_CT\_merge\_L6-10) agreed well, starting with a noticeably high annual growth rate in 2003 and a decreasing period from 2016 to 2018. They only differed considerably in 2008 and 2009, i.e., both CO<sub>2</sub>\_INSITU\_ZSF and CO<sub>2</sub>\_INSITU\_ZSF\_ADVS, but not CO<sub>2</sub>\_CT\_merge\_L6-10, which showed high variations in the annual growth rates. Interestingly, also XCO<sub>2</sub>\_SAT\_merge showed this pattern, which might again be attributed to the different spatiotemporal smoothing in the model and satellite grids compared to the local surface measurements. Especially for the period 2004–2009, it is clear that the annual growth rates in CO<sub>2</sub>\_CT\_merge\_L6-10 remained stable and the same is true for XCO<sub>2</sub>\_CT\_merge\_L1-25.

Regarding column-averaged measurements, smaller variables were expected for the annual growth rates, as shown in Figure 4. Despite much shorter TCCON time-series, the decreasing trends from 2016 to 2018 were still observed in all column-averaged time-series. In 2014, a comparably lower mean annual CO<sub>2</sub> growth rate was depicted across all time-series. Moreover, while the 12 values tended to vary largely in 2017, they did not in 2016 and 2018. Again, this was a result consistent for all seven data sets. However, an increase in growth rates in XCO<sub>2</sub>\_SAT\_merge from 2003 to 2007 was not seen elsewhere and thus still remains unclear. However, in general, annual growth rates agreed well among all CO<sub>2</sub> series, particularly in the second half of the study period, and further research should be dedicated to the differences before 2010.

## 5.2. Correlation of Annual Growth Rates

Figure 6 summarizes correlations of each measurement data set with CO<sub>2</sub>\_INSITU\_ZSF and CO<sub>2</sub>\_INSITU\_ZSF\_ADVS. The ADVS data selection intends to derive more representative CO<sub>2</sub> levels for a broader region, which proved to be valid since the correlation coefficients to CO<sub>2</sub>\_INSITU\_ZSF\_ADVS were higher than the respective ones to CO<sub>2</sub>\_INSITU\_ZSF, e.g., correlation of XCO<sub>2</sub>\_TCCON\_Garmisch growth rates to CO<sub>2</sub>\_INSITU\_ZSF\_ADVS of 0.54 (significant at 0.1 level) instead of 0.38 to CO<sub>2</sub>\_INSITU\_ZSF (not significant). Furthermore, the CarbonTracker models also showed improved correlations from 0.66 to 0.78 with improved significance levels (0.01 to 0.001) for CO<sub>2</sub>\_CT\_merge\_L6-10, and from 0.61 to 0.76 for XCO<sub>2</sub>\_CT\_merge\_L1-25 when applying the ADVS technique. A slight increase (0.57 to 0.62 at 0.05 of the significance level) is also seen for XCO<sub>2</sub>\_sat\_merge, while the highest correlation coefficients of almost 1 were seen for XCO<sub>2</sub>\_TCCON\_Zugspitze in both pairs, however, due to a correlation of three points from only 2015 to 2018, this is not comparable. In short, the overall improvements in the correlation coefficients were clearly recognized in all data sets with continuous in-situ measurements at ZSF after ADVS data selection, suggesting a good accordance with the background levels in the atmosphere. Interestingly, the modeled column time-series correlated better with the surface measurements in terms of the trend compared to other column-averaged measurements. Nevertheless, correlations between CO<sub>2</sub>\_CT\_merge\_L6-10 and continuous in-situ measurements as well as between XCO<sub>2</sub>\_CT\_merge\_L1-25 and column-averaged measurements are also provided (see Figure A2) and especially show a good correlation coefficient (0.82 \*\*) between XCO<sub>2</sub>\_TCCON\_Garmisch and the modeled column data set.

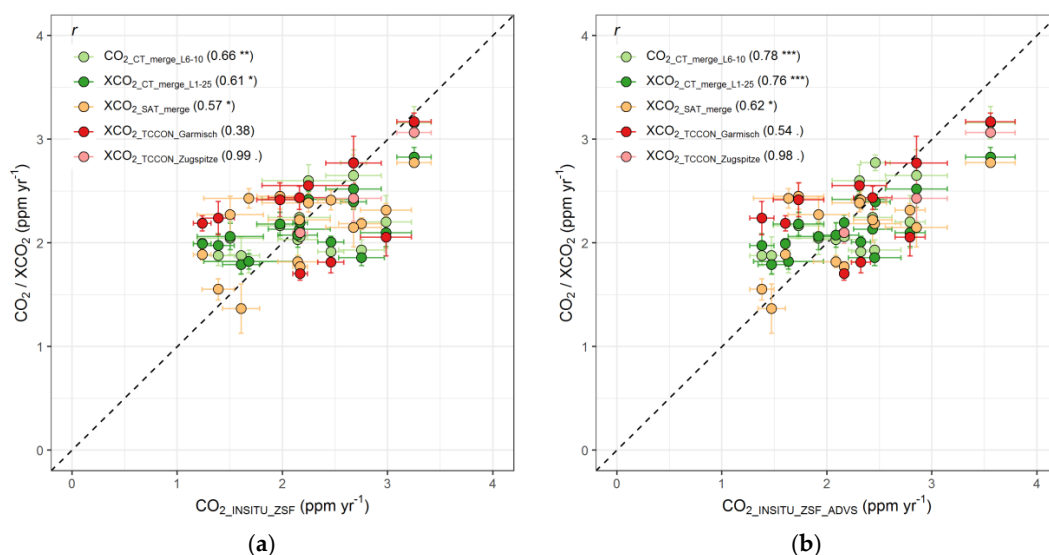


**Figure 6.** Scatter plots of annual mean growth rates from STL trend components in (a) CO<sub>2</sub>\_INSITU\_ZSF and (b) CO<sub>2</sub>\_INSITU\_ZSF\_ADVS versus CO<sub>2</sub>/XCO<sub>2</sub> from other measurement data sets. Pearson's product-moment correlation coefficients ( $r$ ) are listed accordingly for each pair. The significance levels are shown in symbols as 0.001 (\*\*\*), 0.01 (\*\*), 0.05 (\*), and 0.1 (.). The 95% confidence intervals are shown as error bars on both the x and y-axis with dashed lines representing the 1:1 line.

The levels of correlation coefficients were comparable with similar studies. Buchwitz et al. [27] reported a correlation coefficient of 0.82 between the satellite-derived growth rates and the NOAA global growth rates over 2003–2016. This higher value is assumed to be due to the global averaging effect, while our results show a more specific signature of the Zugspitze region. Equally, Schibig et al. [16] reported that correlations between the FTIR and in-situ NDIR measurements, both with and without seasonality, reached 0.82 as well.

### 5.3. Seasonality

The mean seasonal amplitudes of column-averaged measurements were only about one half of the amplitudes of in-situ measurements (see Figure 5). It is noteworthy that this factor-of-two amplitude reduction for column-based data sets was nicely reproduced by CarbonTracker, when comparing  $\text{CO}_2_{\text{CT\_merge\_L6-10}}$  with  $\text{CO}_2_{\text{CT\_merge\_L1-25}}$  ( $6.36 \pm 0.18$  ppm). A similar effect was also reported by Olsen and Randerson [15] for individual NOAA sites in the Northern Hemisphere. The satellite time-series had seasonal amplitudes of  $6.94 \pm 0.22$  ppm from 2003 to 2018, while  $6.58 \pm 0.19$  ppm was calculated for  $\text{XCO}_2_{\text{TCCON\_Garmisch}}$  during 2008–2018. Finally,  $\text{XCO}_2_{\text{TCCON\_Zugspitze}}$  exhibited the lowest mean seasonal amplitude of  $5.22 \pm 0.14$  ppm for the last four years (2015–2018). Taking the same period for the TCCON Garmisch site, the mean seasonal amplitude was still significantly higher ( $6.64 \pm 0.50$  ppm for  $\text{XCO}_2_{\text{TCCON\_Garmisch}}$  during 2015–2018). Therefore, an amplitude difference of around 1.5 ppm can be attributed mainly to the carbon sinks from photosynthesis in the relatively lower elevations of the Zugspitze region compared to the TCCON Zugspitze site (from both the TCCON Garmisch site and the satellite grid coverage perspectives).

In addition, due to different vertical mixing and amounts of air masses measured at the surface or in the column, changes in phase (i.e., timing of seasonal peaks) are expected to be observed as well [7,22]. Olsen and Randerson [15] suggested that the phase delay between surface and column measurements can be up to seven weeks regarding the timing of seasonal maximum and minimum, while Lindqvist et al. [34] showed an up to two–three weeks difference regarding the maximum at the European sites with a smaller difference for the minimum of less than six days. From our study, given that monthly time-series were used, only the shifts in month could be derived here. On average, one–two-month delays were detected in monthly maxima from all column measurements compared to  $\text{CO}_2_{\text{INSITU\_ZSF}}$ , especially in the first half of the satellite time-series ( $\text{XCO}_2_{\text{SAT\_merge}}$ , 2003–2008). Interestingly, the seasonal amplitudes during this period of  $\text{XCO}_2_{\text{SAT\_merge}}$  also differed greatly from the remaining latter half (2009–2018). This could be probably explained by the fact that the TANSO-FTS/GOSAT satellite measurements included in this merged product ( $\text{XCO}_2_{\text{SAT\_Obs4MIPs}}$ ) only started from 2009. In opposition to this, delays of one month at the most can be found for seasonal minima mainly from satellite and TCCON measurements.

At last, inter-annual changes in the seasonality were detected more clearly for continuous in-situ measurements than for the column-averaged measurements, which is in accordance with the anomalies described in Section 4.1. However, some other seasonal patterns are still worthy of further investigations. A slight “shoulder” behavior could be observed for all time-series, usually around November and December, suggesting a slower  $\text{CO}_2$  increase during this period. Such a “pause” cannot be fully understood yet, but is probably associated with a known, relatively regular winter warming effect (named “Christmas-thaw weather” over Europe). Meanwhile, the seasonal decrease from monthly maximum to monthly minimum tended to vary rapidly over time, indicating the great influences from vegetation photosynthesis as the carbon sinks during spring to summertime. Such a pattern should be described more precisely in seasonal modeling in the future.

## 6. Conclusions

This study compared surface  $\text{CO}_2$  measurements with column-averaged measurements at a specific site in Southern Germany. Continuous in-situ  $\text{CO}_2$  measurements from 2002 to 2018 at Zugspitze–Schneefernerhaus were used and selected by the data selection method ADVS in order

to obtain more representative background levels for a broader region. In order to compare with ground-based FTIR measurements, two TCCON sites, Garmisch and Zugspitze, were chosen at the nearby locations. In addition to providing more comparable results over the region, satellite measurements were included by defining selected grids centered at the specific Zugspitze site. At last, the simulated CO<sub>2</sub> mole fractions from the CarbonTracker models were included and validated for other measurements.

The mean offsets of satellite and FTIR measurements from the continuous in-situ measurements were less than 2.0 ppm, showing generally good agreements. By decomposing each CO<sub>2</sub> time-series into trend, seasonal, and remainder components, the annual growth rates and seasonal amplitudes were compared. Fluctuations of the mean annual growth rates were consistent over the time period, proving that both continuous in-situ and column-averaged measurements are able to capture the CO<sub>2</sub> trend effectively in the atmosphere. The correlation analysis showed lower correlation coefficients than other global studies due to the site-specific focus of this study. However, differences in seasonal cycles were clear with respect to both amplitudes and phases. Column-averaged measurements exhibited smaller seasonal amplitudes and clearly delayed phases regarding both seasonal maximum and minimum. This is most likely due to lessened influences from the local to regional scale as well as to a time lag by the vertical mixing of greater amounts of air masses in the column profile.

With respect to the research questions, the study clearly showed that different types of CO<sub>2</sub> measurements/time-series are comparable by applying a consistent data processing routine. The main differences between continuous in-situ and column-averaged measurements were detected in the seasonal amplitudes, supporting the essential distinction of the measuring objects. However, potential errors should always be noted, especially regarding both temporal and spatial resolutions. Such a comparison provides the basis for a better understanding of these two different types of measurements and is helpful for improved data integration in further research.

**Author Contributions:** The research aim was developed by Y.Y., L.R., and A.M.; Formal analysis, methodology, and implementation of the programming algorithm were done by Y.Y. under the supervision of L.R., H.P., R.S., and A.M.; The ground-based FTS measurements were performed and collected by R.S. and M.R.; The original draft was prepared by Y.Y. and reviewed and edited by all co-authors.

**Funding:** Y.Y. is funded by the China Scholarship Council (CSC), grant number 201508080110.

**Acknowledgments:** We acknowledge support from a MICMoR fellowship through the KIT/IMK-IFU to Ye Yuan. The Obs4MIPs XCO<sub>2</sub> satellite data have been obtained from the Copernicus Climate Change Service (C3S) Climate Data Store (<https://cds.climate.copernicus.eu/>). We thank Michael Buchwitz, University of Bremen, for providing comments on an early draft of this manuscript. OCO-2 satellite data products were produced by the OCO-2 project at the Jet Propulsion Laboratory, California Institute of Technology, and obtained from the OCO-2 data archive maintained at the NASA Goddard Earth Science Data and Information Services Center. CarbonTracker CT2017 and CT-NRT.v2018-1 results were provided by NOAA ESRL, Boulder, Colorado, USA from the website at <http://carbontracker.noaa.gov>.

**Conflicts of Interest:** The authors declare no conflict of interest.

## Appendix A

## Figures

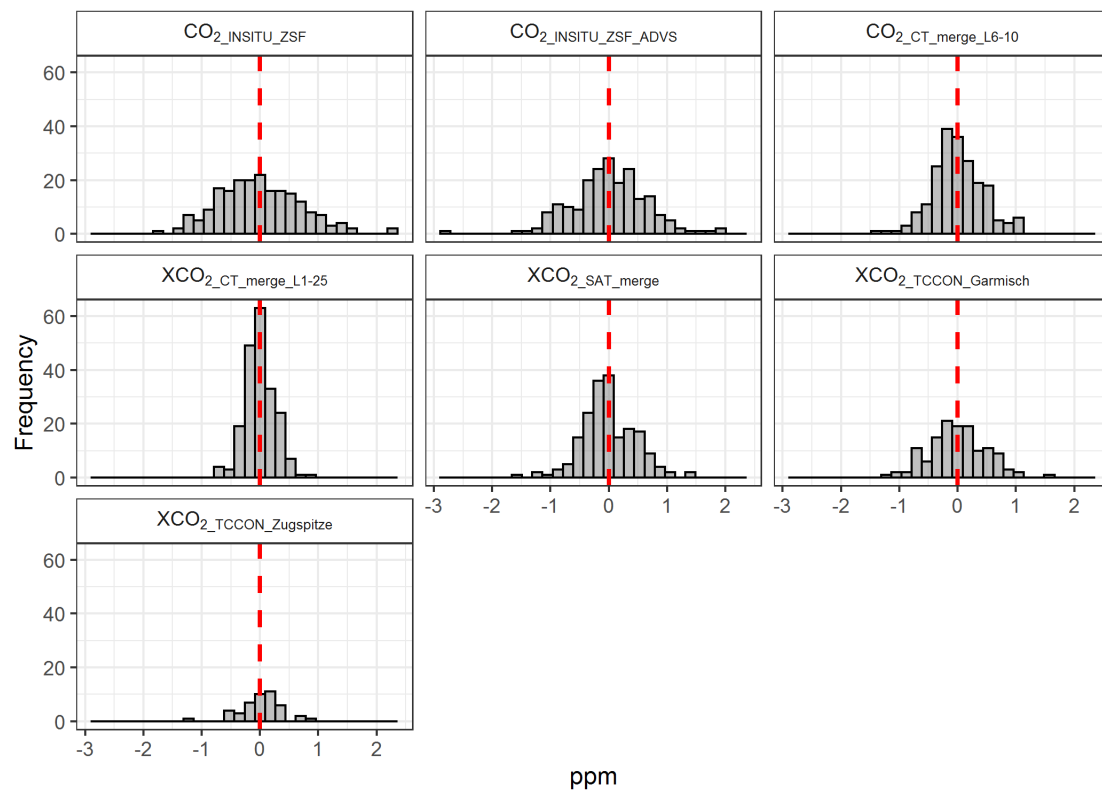


**Figure A1.** Histogram of STL-decomposed remainder components from all CO<sub>2</sub> and XCO<sub>2</sub> data sets of this study. Red dashed line shows the mean of each distribution.

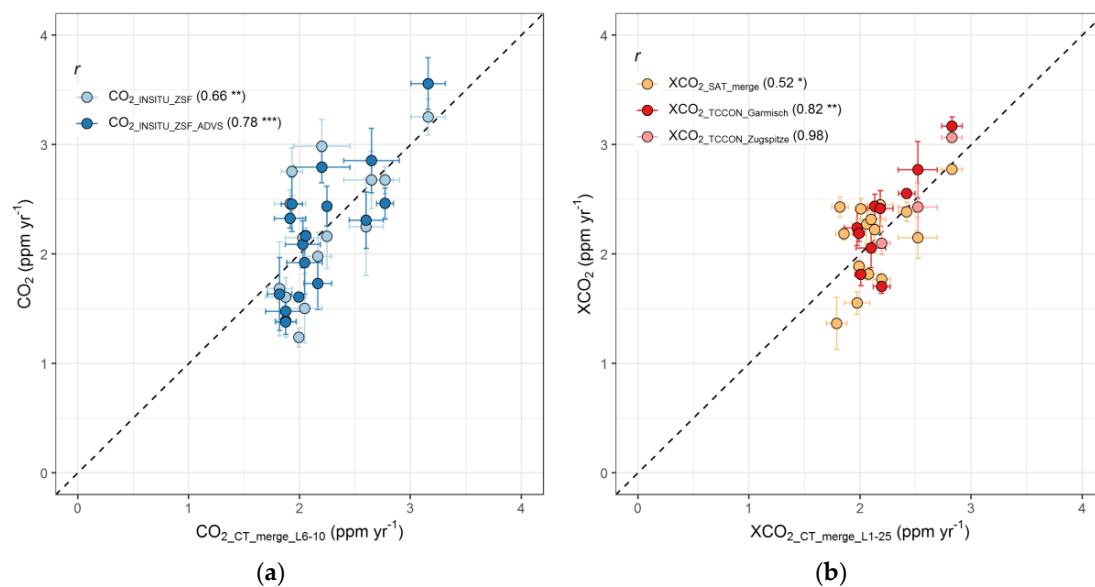


**Figure A2.** Scatter plots of annual mean growth rates from STL trend components in (a) CO<sub>2</sub>\_CT\_merge\_L6-10 and (b) XCO<sub>2</sub>\_CT\_merge\_L1-25 versus CO<sub>2</sub>/XCO<sub>2</sub> measurements. Pearson's product-moment correlation coefficients ( $r$ ) are listed accordingly for each pair. The significance levels are shown in symbols as 0.001 (\*\*\*), 0.01 (\*\*), and 0.05 (\*). The 95% confidence intervals are shown as error bars on both x- and y-axis with dashed lines representing the 1:1 line.



Table

**Table A1.** Statistical summary of all CO<sub>2</sub> and XCO<sub>2</sub> data sets in this study.

Measurement Technique	Offset from CO <sub>2</sub> <sub>insitu_ZSF</sub> (ppm ± 95% CI)	Mean Annual Growth Rate (ppm yr <sup>-1</sup> ± 95% CI)	Mean Seasonal Amplitude (ppm ± 95% CI)
CO <sub>2</sub> <sub>INSITU_ZSF</sub>	–	2.18 ± 0.10	13.08 ± 0.52
CO <sub>2</sub> <sub>INSITU_ZSF_ADV5</sub>	−0.66 ± 0.15	2.20 ± 0.09	10.93 ± 0.45
CO <sub>2</sub> <sub>CT_merge_L6-10</sub>	0.01 ± 0.17	2.21 ± 0.06	11.05 ± 0.28
XCO <sub>2</sub> <sub>CT_merge_L1-25</sub>	−2.36 ± 0.32	2.15 ± 0.04	6.36 ± 0.18
XCO <sub>2</sub> <sub>SAT_merge</sub>	−1.17 ± 0.38	2.13 ± 0.06	6.94 ± 0.22
XCO <sub>2</sub> <sub>TCCON_Garmisch</sub>	−1.95 ± 0.43	2.33 ± 0.08	6.58 ± 0.19
XCO <sub>2</sub> <sub>TCCON_Zugspitze</sub>	−1.03 ± 1.01	2.48 ± 0.16	5.22 ± 0.14

### Comparison of Data Processing Methods

While it is aimed in this study to examine the applicability of the consistent data processing routine to various types of CO<sub>2</sub> measurements, the performance on the column-averaged measurements is focused here since the data processing routine has been applied practically to continuous in-situ measurements in other studies (e.g., [7,22]). Therefore, a re-processing on the same column-averaged data set (XCO<sub>2</sub><sub>TCCON\_Garmisch</sub>) used in Lindqvist et al. [34] but for a different time period (May/2009–Oct/2013) was performed and compared here. The reference study applied a skewed sine wave for the seasonal cycle with an upward linear trend in the following function

$$f(t) = a_0 + a_1 t + a_2 \sin(\omega[t - a_3] + \cos^{-1}[a_4 \cos(\omega[t - a_5])])$$

where  $a_1$  indicates the CO<sub>2</sub> growth rate in trend and  $2|a_2|$  denotes the peak-to-peak amplitude for the seasonal cycle. The XCO<sub>2</sub><sub>TCCON\_Garmisch</sub> data subset for the corresponding time period was extracted and decomposed by STL again and resulted in a mean annual growth rate of  $2.12 \pm 0.11$  ppm yr<sup>-1</sup>, and a mean seasonal amplitude of  $6.56 \pm 0.27$  ppm. Compared to the reference results ( $2.03 \pm 0.04$  ppm yr<sup>-1</sup> and  $6.6 \pm 0.1$  ppm, respectively), good agreements have been reached. However, small errors can be seen in the reference as daily XCO<sub>2</sub> values were included in the fitted function, while only monthly averaged data sets were used here. Also note that with the fitted sine term, a lack of data would play a minor role in determining the seasonal amplitude. In this case, XCO<sub>2</sub> data in 2009 cannot contribute to the mean seasonal amplitude because this data subset starts in May and the monthly maximum is assumed to be missing so that no seasonal amplitude can be calculated. Nevertheless, inter-annual variations cannot be derived from the function-fitted parameters, which help substantially in evaluating the performance of consistent data processing routines in our study.

### References

1. IPCC. Climate Change 2014: Synthesis Report. In *Contribution of Working Groups I, II and III to the Fifth Assessment Report of the Intergovernmental Panel on Climate Change*; Pachauri, R.K., Meyer, L.A., Eds.; Core Writing Team: Geneva, Switzerland, 2014; p. 151. ISBN 978-929-169-143-2.
2. Dlugokencky, E.; Tans, P. Trends in Atmospheric Carbon Dioxide. NOAA/ESRL. Available online: [www.esrl.noaa.gov/gmd/ccgg/trends/](http://www.esrl.noaa.gov/gmd/ccgg/trends/) (accessed on 21 October 2019).
3. Schultz, M.G.; Akimoto, H.; Bottenheim, J.; Buchmann, B.; Galbally, I.E.; Gilge, S.; Helmig, D.; Koide, H.; Lewis, A.C.; Novelli, P.C.; et al. The Global Atmosphere Watch reactive gases measurement network. *Elem. Sci. Anthr.* **2015**, *3*. [[CrossRef](#)]
4. Toon, G.; Blavier, J.; Washenfelder, R.; Wunch, D.; Keppel-Aleks, G.; Wennberg, P.; Connor, B.; Sherlock, V.; Griffith, D.; Deutscher, N.; et al. Total Column Carbon Observing Network (TCCON). In *Advances in Imaging, OSA Technical Digest (CD)*. *Opt. Soc. Am.* **2009**, JMA3. [[CrossRef](#)]
5. Hamazaki, T.; Kaneko, Y.; Kuze, A.; Kondo, K. Fourier transform spectrometer for Greenhouse Gases Observing Satellite (GOSAT). *Enabling Sens. Platf. Technol. Spaceborne Remote Sens.* **2005**, *5659*, 73–80. [[CrossRef](#)]

6. Crisp, D. Measuring atmospheric carbon dioxide from space with the Orbiting Carbon Observatory-2 (OCO-2). *Earth Obs. Syst.* **2015**, *9607*, 960702. [[CrossRef](#)]
7. Yuan, Y.; Ries, L.; Petermeier, H.; Steinbacher, M.; Gómez-Peláez, A.J.; Leuenberger, M.C.; Schumacher, M.; Trickl, T.; Couret, C.; Meinhardt, F.; et al. Adaptive selection of diurnal minimum variation: A statistical strategy to obtain representative atmospheric CO<sub>2</sub> data and its application to European elevated mountain stations. *Atmos. Meas. Tech.* **2018**, *11*, 1501–1514. [[CrossRef](#)]
8. Fang, S.X.; Zhou, L.X.; Tans, P.P.; Ciais, P.; Steinbacher, M.; Xu, L.; Luan, T. In situ measurement of atmospheric CO<sub>2</sub> at the four WMO/GAW stations in China. *Atmos. Chem. Phys.* **2014**, *14*, 2541–2554. [[CrossRef](#)]
9. Hernández-Paniagua, I.Y.; Lowry, D.; Clemitshaw, K.C.; Fisher, R.E.; France, J.L.; Lanoisellé, M.; Ramonet, M.; Nisbet, E.G. Diurnal, seasonal, and annual trends in atmospheric CO<sub>2</sub> at southwest London during 2000–2012: Wind sector analysis and comparison with Mace Head, Ireland. *Atmos. Environ.* **2015**, *105*, 138–147. [[CrossRef](#)]
10. Burrows, J.P.; Hölzle, E.; Goede, A.P.H.; Visser, H.; Fricke, W. SCIAMACHY—scanning imaging absorption spectrometer for atmospheric cartography. *Acta Astronaut.* **1995**, *35*, 445–451. [[CrossRef](#)]
11. Bovensmann, H.; Burrows, J.P.; Buchwitz, M.; Frerick, J.; Noël, S.; Rozanov, V.V.; Chance, K.V.; Goede, A.P.H. SCIAMACHY: Mission Objectives and Measurement Modes. *J. Atmos. Sci.* **1999**, *56*, 127–150. [[CrossRef](#)]
12. Aumann, H.H.; Miller, C.R. Atmospheric infrared sounder (AIRS) on the earth observing system. *Adv. Next Gener. Satell.* **1995**, *2583*, 332–343. [[CrossRef](#)]
13. Miao, R.; Lu, N.; Yao, L.; Zhu, Y.; Wang, J.; Sun, J. Multi-Year Comparison of Carbon Dioxide from Satellite Data with Ground-Based FTS Measurements (2003–2011). *Remote Sens.* **2013**, *5*, 3431–3456. [[CrossRef](#)]
14. Liang, A.; Gong, W.; Han, G.; Xiang, C. Comparison of Satellite-Observed XCO<sub>2</sub> from GOSAT, OCO-2, and Ground-Based TCCON. *Remote Sens.* **2017**, *9*, 1033. [[CrossRef](#)]
15. Olsen, S.C.; Randerson, J.T. Differences between surface and column atmospheric CO<sub>2</sub> and implications for carbon cycle research. *J. Geophys. Res.* **2004**, *109*, 419. [[CrossRef](#)]
16. Schibig, M.F.; Mahieu, E.; Henne, S.; Lejeune, B.; Leuenberger, M.C. Intercomparison of in situ NDIR and column FTIR measurements of CO<sub>2</sub> at Jungfraujoch. *Atmos. Chem. Phys.* **2016**, *16*, 9935–9949. [[CrossRef](#)]
17. Shim, C.; Lee, J.; Wang, Y. Effect of continental sources and sinks on the seasonal and latitudinal gradient of atmospheric carbon dioxide over East Asia. *Atmos. Environ.* **2013**, *79*, 853–860. [[CrossRef](#)]
18. Nalini, K.; Uma, K.N.; Sijikumar, S.; Tiwari, Y.K.; Ramachandran, R. Satellite- and ground-based measurements of CO<sub>2</sub> over the Indian region: Its seasonal dependencies, spatial variability, and model estimates. *Int. J. Remote Sens.* **2018**, *39*, 7881–7900. [[CrossRef](#)]
19. Sánchez, M.L.; Pérez, I.A.; Buchwitz, M.; García, M.A. XCO<sub>2</sub> SCIAMACHY Total Column and CO<sub>2</sub> Ground Inter-comparison Results in the Spanish Plateau. In *Proceedings of the ESA Living Planet Symposium, Bergen, Norway, 28 June–2 July 2010*; Lacoste-Francis, H., Ed.; ESA Communications: Noordwijk, The Netherlands, 2010; ISBN 978-929-221-250-6.
20. Warneke, T.; Yang, Z.; Olsen, S.; Körner, S.; Notholt, J.; Toon, G.C.; Velasco, V.; Schulz, A.; Schrems, O. Seasonal and latitudinal variations of column averaged volume-mixing ratios of atmospheric CO<sub>2</sub>. *Geophys. Res. Lett.* **2005**, *32*, L03808. [[CrossRef](#)]
21. Warneke, T.; Petersen, A.K.; Gerbig, C.; Jordan, A.; Rödenbeck, C.; Rothe, M.; Macatangay, R.; Notholt, J.; Schrems, O. Co-located column and in situ measurements of CO<sub>2</sub> in the tropics compared with model simulations. *Atmos. Chem. Phys.* **2010**, *10*, 5593–5599. [[CrossRef](#)]
22. Yuan, Y.; Ries, L.; Petermeier, H.; Trickl, T.; Leuchner, M.; Couret, C.; Sohmer, R.; Meinhardt, F.; Menzel, A. On the diurnal, weekly, and seasonal cycles and annual trends in atmospheric CO<sub>2</sub> at Mount Zugspitze, Germany, during 1981–2016. *Atmos. Chem. Phys.* **2019**, *19*, 999–1012. [[CrossRef](#)]
23. Wunch, D.; Toon, G.C.; Blavier, J.F.L.; Washenfelder, R.A.; Notholt, J.; Connor, B.J.; Griffith, D.W.T.; Sherlock, V.; Wennberg, P.O. The total carbon column observing network. *Philos. Trans. A Math. Phys. Eng. Sci.* **2011**, *369*, 2087–2112. [[CrossRef](#)]
24. Sussmann, R.; Schäfer, K. Infrared spectroscopy of tropospheric trace gases: Combined analysis of horizontal and vertical column abundances. *Appl. Opt.* **1997**, *36*, 735–741. [[CrossRef](#)] [[PubMed](#)]
25. Sussmann, R.; Rettinger, M. TCCON Data from Zugspitze (DE), Release GGG2014.R1 [Data set]. *CaltechDATA* **2018**, *r1*. [[CrossRef](#)]
26. Sussmann, R.; Rettinger, M. TCCON data from Garmisch (DE), Release GGG2014.R2 [Data set]. *CaltechDATA* **2018**, *r2*. [[CrossRef](#)]

27. Buchwitz, M.; Reuter, M.; Schneising, O.; Noël, S.; Gier, B.; Bovensmann, H.; Burrows, J.P.; Boesch, H.; Anand, J.; Parker, R.J.; et al. Computation and analysis of atmospheric carbon dioxide annual mean growth rates from satellite observations during 2003–2016. *Atmos. Chem. Phys.* **2018**, *18*, 17355–17370. [[CrossRef](#)]
28. Crisp, D.; Pollock, H.R.; Rosenberg, R.; Chapsky, L.; Lee, R.A.M.; Oyafuso, F.A.; Frankenberg, C.; O'Dell, C.W.; Bruegge, C.J.; Doran, G.B.; et al. The on-orbit performance of the Orbiting Carbon Observatory-2 (OCO-2) instrument and its radiometrically calibrated products. *Atmos. Meas. Tech.* **2017**, *10*, 59–81. [[CrossRef](#)]
29. Peters, W.; Jacobson, A.R.; Sweeney, C.; Andrews, A.E.; Conway, T.J.; Masarie, K.; Miller, J.B.; Bruhwiler, L.M.P.; Pétron, G.; Hirsch, A.I.; et al. An atmospheric perspective on North American carbon dioxide exchange: CarbonTracker. *Proc. Natl. Acad. Sci. USA* **2007**, *104*, 18925–18930. [[CrossRef](#)]
30. Buschmann, M.; Deutscher, N.M.; Sherlock, V.; Palm, M.; Warneke, T.; Notholt, J. Retrieval of XCO<sub>2</sub> from ground-based mid-infrared (NDACC) solar absorption spectra and comparison to TCCON. *Atmos. Meas. Tech.* **2016**, *9*, 577–585. [[CrossRef](#)]
31. Berrisford, P.; Dee, D.P.; Poli, P.; Brugge, R.; Fielding, M.; Fuentes, M.; Kållberg, P.W.; Kobayashi, S.; Uppala, S.; Simmons, A. The ERA-Interim archive Version 2.0. ERA Report, ECMWF. 2011, p. 23. Available online: <https://www.ecmwf.int/node/8174> (accessed on 31 October 2019).
32. Cleveland, R.B.; Cleveland, W.S.; McRae, J.E.; Terpenning, I. STL: A seasonal-trend decomposition. *J. Off. Stat.* **1990**, *6*, 3–73.
33. Pickers, P.A.; Manning, A.C. Investigating bias in the application of curve fitting programs to atmospheric time series. *Atmos. Meas. Tech.* **2015**, *8*, 1469–1489. [[CrossRef](#)]
34. Lindqvist, H.; O'Dell, C.W.; Basu, S.; Boesch, H.; Chevallier, F.; Deutscher, N.; Feng, L.; Fisher, B.; Hase, F.; Inoue, M.; et al. Does GOSAT capture the true seasonal cycle of carbon dioxide? *Atmos. Chem. Phys.* **2015**, *15*, 13023–13040. [[CrossRef](#)]
35. RC Team. R: A Language and Environment for Statistical Computing; Vienna, Austria. 2014. Available online: <https://www.R-project.org/> (accessed on 11 December 2019).
36. Dowle, M.; Srinivasan, A. Data. Table: Extension of 'Data.Frame'. 2019. Available online: <https://CRAN.R-project.org/package=data.table> (accessed on 9 December 12).
37. Carslaw, D.C.; Ropkins, K. openair—An R package for air quality data analysis. *Environ. Model. Softw.* **2012**, *27–28*, 52–61. [[CrossRef](#)]
38. Zeileis, A.; Grothendieck, G. Zoo: S3 Infrastructure for Regular and Irregular Time Series. *J. Stat. Softw.* **2005**, *14*, 1–27. [[CrossRef](#)]
39. Wickham, H. *Ggplot2: Elegant Graphics for Data Analysis*; Springer-Verlag: New York, NY, USA, 2016; ISBN 978-331-924-277-4.
40. Cheng, J.; Karambelkar, B.; Xie, Y. Leaflet: Create Interactive Web Maps with the JavaScript 'Leaflet' Library. 2018. Available online: <https://CRAN.R-project.org/package=leaflet> (accessed on 16 November 2019).
41. Appelhans, T.; Detsch, F.; Reudenbach, C.; Woellauer, S. Mapview: Interactive Viewing of Spatial Data in R. 2019. Available online: <https://CRAN.R-project.org/package=mapview> (accessed on 13 May 2019).
42. Auguie, B. Gridextra: Miscellaneous Functions for "Grid" Graphics. 2017. Available online: <https://CRAN.R-project.org/package=gridExtra> (accessed on 9 September 2017).
43. Heymann, J.; Reuter, M.; Buchwitz, M.; Schneising, O.; Bovensmann, H.; Burrows, J.P.; Massart, S.; Kaiser, J.W.; Crisp, D. CO<sub>2</sub> emission of Indonesian fires in 2015 estimated from satellite-derived atmospheric CO<sub>2</sub> concentrations. *Geophys. Res. Lett.* **2017**, *44*, 1537–1544. [[CrossRef](#)]
44. Liu, J.; Bowman, K.W.; Schimel, D.S.; Parazoo, N.C.; Jiang, Z.; Lee, M.; Bloom, A.A.; Wunch, D.; Frankenberg, C.; Sun, Y.; et al. Contrasting carbon cycle responses of the tropical continents to the 2015–2016 El Niño. *Science* **2017**, *358*. [[CrossRef](#)]
45. Peters, G.P.; Le Quéré, C.; Andrew, R.M.; Canadell, J.G.; Friedlingstein, P.; Ilyina, T.; Jackson, R.B.; Joos, F.; Korsbakken, J.I.; McKinley, G.A.; et al. Towards real-time verification of CO<sub>2</sub> emissions. *Nat. Clim. Chang.* **2017**, *7*, 848. [[CrossRef](#)]

